# Nonlinear Least Squares Estimation for Breathing Monitoring Using FMCW Radars

Gabriel Beltrão[#1], Mohammad Alaee-Kerahroodi[#], Udo Schroeder[*] Dimitri Tatarinov[*] Bhavani Shankar M.R.[#]

[#]SnT - Interdisciplinary Centre for Security, Reliability and Trust, University of Luxembourg, Luxembourg

[*]IEE S.A., Luxembourg

[1]gabriel.tedgue-beltrao@uni.lu

***Abstract* — In this paper we propose a novel framework for breathing monitoring, based on a simple Nonlinear Least Squares (NLS) estimation, which explores the harmonic structure of the breathing displacement signal. The first part of the study was performed using a controlled target which could be programmed for executing breathing-like movements, thus emulating the chest-wall displacement over time. Finally, the proposed approach was evaluated with real human data, and the results have shown robust and accurate estimation, outperforming previous methods over different scenarios.**

***Keywords* — vital-signs, breathing, radar, FMCW.**

## I. Introduction

The non-contact monitoring of the cardiorespiratory activity provides several advantages over standard devices. It neither confines nor inhibits the subject, and does not cause any discomfort, skin damage or irritation as electrodes, adhesive sensors or straps could do [1]. This is especially important in the case of newborns and people with sensitive skin, as well as for long-term monitoring.

The activity of the cardiovascular and respiratory systems causes some physical and physiological effects on the human body. The chest-wall moves during the inspiration/expiration cycle as a result of the diaphragm muscle movement. These small and periodic movements can be detected by the radar, allowing accurate estimation of breathing rates in certain conditions. However, due to the reduced amplitudes, the backscattered signal can be easily buried in the background noise, or masked by strong interference arising from the external environment.

In this paper we present our preliminary experimental results with breathing detection and estimation using a commercial Frequency-Modulated Continuous-Wave (FMCW) device. The first part of the study was performed using a controlled target which could be programmed for executing breathing-like movements, thus emulating the chest-wall displacement over time. Subsequently, we propose a novel framework for breathing monitoring, based on a simple Nonlinear Least Squares (NLS) estimation, which explores the harmonic structure of the breathing displacement signal, and is asymptotically efficient for large time windows. The proposed approach is evaluated with real human data in different scenarios, and its performance is compared to conventional Discrete Fourier Transform (DFT) estimation and Frequency-Time Phase Regression (FTPR) techniques [2].

The remainder of this paper is organized as follows. In section II, we introduce the signal model and problem formulation for breathing detection using FMCW radars. The system framework for signal processing and estimation is proposed in Section III, while Section IV presents our experimental results. Finally, in Section V, some conclusions are drawn.

## II. Problem Formulation

The received FMCW signal is a scaled and time-shifted version of the transmitted signal, in which the phase variation across received pulses contains the information about the target's movement. Assuming no range migration during the coherent processing interval (CPI), the slow-time phase variation at the target range bin can be written as

$$\Delta\theta(t) = \frac{4\pi x(t)}{\lambda}, \tag{1}$$

where $\lambda$ is the operating wavelength, and $x(t)$ is the slow-time displacement signal containing the periodic chest-wall movement due to the breathing. Many different methods have already been proposed for modeling $x(t)$, from simple sinusoidal approximations, to more complicated patterns as described in [3]. In any case, due to the periodic nature of breathing, any function representing this movement can eventually be decomposed into Fourier terms containing the fundamental frequencies and harmonics corresponding to the breathing rates we aim to estimate, i.e., the displacement signal $x(n)$ can be modeled as a sum of $L_k$ harmonically related complex sinusoids, having frequencies that are integer multiples of a fundamental frequency $w_k > 0$. Such a signal can be written for $n = 0, ..., N-1$ as [4]

$$x(n) = \sum_{k=1}^{K} x_k(n) = \sum_{k=1}^{K}\sum_{l=1}^{L_k} a_{k,l} e^{jw_k ln}, \tag{2}$$

where $a_{k,l} = A_{k,l}e^{j\phi_{k,l}}$ is the complex amplitude of the $l$th harmonic, $L_k$ represents the number of harmonics (the model order), and $K$ refers to the number of sources (scatters). This allows for modelling different scatters over the chest-wall and belly, not only for the breathing, but also for the heartbeat movement. In this work, we are considering only a single breathing scatter, i.e. $K = 1$. For healthy adults, standard amplitude values for the breathing movement are in the range



Authorized licensed use limited to: Technische Informationsbibliothek (TIB). Downloaded on April 04,2025 at 12:10:30 UTC from IEEE Xplore. Restrictions apply.

of 4 mm to 12 mm, while breathing rates can vary from 5 to 30 breaths per minute (bpm) [3].

It is useful to define $\boldsymbol{x}_k = [\ x_k(0)\ ...\ x_k(N-1)\ ]^T \in \mathbb{C}^N$, the vector consisting of $N$ consecutive samples of $x_k(n)$, which can be expressed as [5]

$$\boldsymbol{x}_k = \boldsymbol{Z}_k \boldsymbol{a}_k, \tag{3}$$

with $\boldsymbol{a}_k = [\ A_{k,1}e^{j\phi_{k,1}}\ ...\ A_{k,L_k}e^{j\phi_{k,L_k}}\ ]$ being the vector containing the harmonics complex amplitudes, and the matrix $\boldsymbol{Z}_k \in \mathbb{C}^{N\times L_k}$ having a Vandermonde structure, being constructed from the $L_k$ complex sinusoidal vectors as

$$\boldsymbol{Z}_k = [\ \boldsymbol{z}(w_k)\ \boldsymbol{z}(w_k 2)\ ...\ \boldsymbol{z}(w_k L_k)\ ], \tag{4}$$

with $\boldsymbol{z}(w) = [\ 1\ e^{jw}\ ...\ e^{jw(N-1)}\ ]^T$.

## III. Framework for Breathing Monitoring

For these experiments, we are using a Texas Instruments (TI) mm-wave FMCW radar (AWR1642 [6]), operating at 77 GHz with a 4 GHz bandwidth. As we are only considering single-target scenarios, the radar is configured using a single transmit (TX) and receiver (RX) antenna pair. The total duration of each chirp is 64 $\mu s$, with an inter-frame period of 10 $ms$, corresponding to a slow-time sampling frequency of 100 $Hz$. For providing sufficient integration time, while still preserving the update rate, the data is processed using overlapped sliding windows with a duration of 15 seconds and 13 seconds of overlap. This allows enough time for acquiring several breathing cycles, increasing the Signal to Noise Ratio (SNR) and the frequency resolution, but still being able to track fast changes in the breathing rate.

The sampled beat signals, corresponding to the transmitted pulses in each CPI, are rearranged into a matrix format, and undergo a two-dimensional DFT. The resulting range-Doppler map is the input to the detector, responsible for identifying possible range bins containing moving targets (with the desired breathing information). Finally, the output of the range DFT, at the detected range bins, will be used for the estimation process in the subsequent steps.

The complex slow-time signal, from the selected target range bin needs to be further processed in order to obtain the chest-wall displacement over time. Before extracting the desired phase information, possible DC offsets must be compensated. Despite the high range resolution provided by FMCW devices, DC terms originating from other sources (other than the actual chest-wall movement) may eventually be present in the target range bin, and therefore should be corrected. For this, we are using the Levenberg–Marquardt (LM) algorithm, which provides a maximum likelihood estimate to this problem [7].

For enabling precise phase recovery, the arctangent demodulation (AD) [8] is being used. From (1), the displacement signal can be recovered as

$$x(t) = \frac{\lambda}{4\pi} \cdot unwrap\left( \arctan\left[ \frac{\Delta\theta_Q(t)}{\Delta\theta_I(t)} \right] \right). \tag{5}$$

The unwrap operation is necessary for removing possible phase discontinuities caused by the restricted domain of the arctangent function. Due to the high sensitivity of mm-wave devices, wrapped phases around $[-\pi, \pi]$ are expected when actual displacements are greater than $\lambda/4$. The recovered displacement signal is then filtered with a passband FIR Kaiser window ($\beta = 6.5$), from 0.1 Hz to 3 Hz, which includes the range of breathing frequencies and possible harmonics. After this, for highlighting the signal periodicity, and improving the SNR, we calculate the autocorrelation function of filtered signal which will then be used in the final estimation block.

### A. NLS Estimation

The final processing stage is the estimator, which is first performed in time domain. An initial (coarse) estimation is obtained through a peak detection algorithm, applied directly over the pre-processed autocorrelation sequence. Additionally, for better exploring the harmonic structure of the breathing displacement signal (kindly refer to (2)), we propose a simple NLS estimator, which is asymptotically efficient (attains the CRLB) for large time windows (large $N$), even in colored noise [4].

For convenience, let us first define the estimator input vector $\boldsymbol{s} = [\ s(0)\ ...\ s(N-1)\ ]^T \in \mathbb{C}^N$. The NLS estimates are obtained by minimizing the difference between $\boldsymbol{s}$ and the signal model, i.e.,

$$\hat{w}_k = \arg\min_{w_k, \boldsymbol{a}_k} ||\boldsymbol{s} - \boldsymbol{Z}_k \boldsymbol{a}_k||_2^2. \tag{6}$$

Minimizing (6) with respect to the complex amplitudes $\boldsymbol{a}_k$ gives estimates $\hat{\boldsymbol{a}_k} = (\boldsymbol{Z}_k^H \boldsymbol{Z}_k)^{-1} \boldsymbol{Z}_k^H \boldsymbol{s}$, which, when reinserted into (6), lead to [5]

$$\hat{w}_k = \arg\max_{w_k} \boldsymbol{s}^H \boldsymbol{Z}_k (\boldsymbol{Z}_k^H \boldsymbol{Z}_k)^{-1} \boldsymbol{Z}_k^H \boldsymbol{s} \tag{7}$$

$$\approx \arg\max_{w_k} ||\boldsymbol{Z}_k^H \boldsymbol{s}||_2^2, \tag{8}$$

where the last line follows from the assumption that $N \gg 1$. The resulting cost function can be efficiently implemented with a linear grid search using the Fast Fourier Transform (FFT) algorithm, where the estimator reduces to a summation over the power spectral density of $\boldsymbol{s}$. The model order was empirically chosen to be $L_k = 3$. To avoid strong low-frequency components which may eventually be present in real data, the search range was limited to the region within $\pm 5$ bpm around the initial obtained estimation. This strategy also reduces the computational effort to perform the grid search.

## IV. Experimental Results

The first part of the study was performed using a controlled target which could be programmed for executing breathing-like movements, thus emulating the chest-wall displacement over time. The objective was to select the appropriate demodulation algorithms and parameters, in order be able to precise recover the displacement signal. Finally, for validating the complete signal processing chain, human tests were also performed in a laboratory environment. The next subsections will describe each one of the aforementioned scenarios.


Authorized licensed use limited to: Technische Informationsbibliothek (TIB). Downloaded on April 04,2025 at 12:10:30 UTC from IEEE Xplore. Restrictions apply.

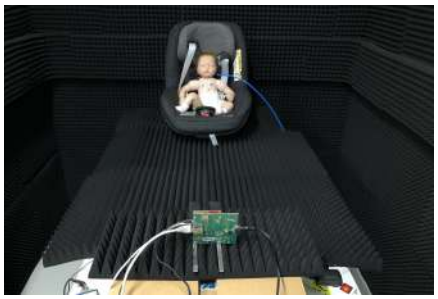

Fig. 1. Setup for the tests with the live dummy. The pump is hidden on the right side.

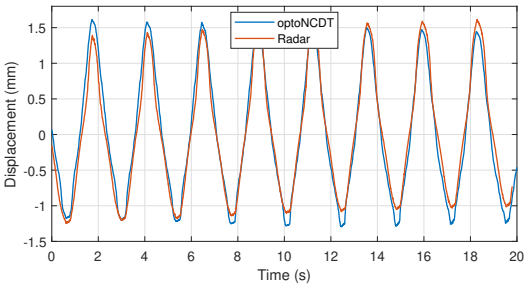


Fig. 2. Recovered displacement signal from the live dummy test.

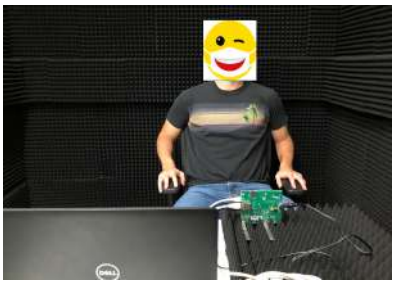

Fig. 3. Setup for the tests with humans.

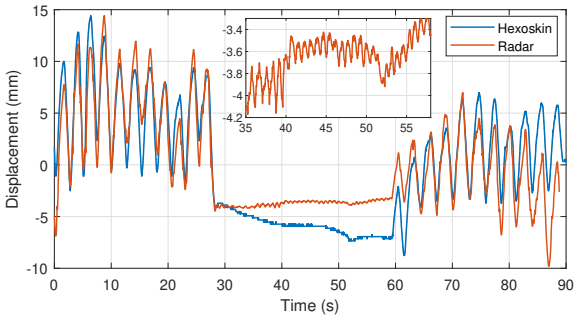


Fig. 4. Chest-wall displacement over time during the hold and release test.

### A. *Live Dummy Tests*

In order to emulate the complex movement of a real target, the first set of tests was performed using a live dummy, developed for repetitive testing of breathing detection in a realistic scenario [9]. The size of the dummy is comparable to newborns, and the torso tissue consists of a radar reflective material, integrated to a vacuum pump, which excites the torso to contract and expand cyclically. For providing ground-truth information regarding the actual movement, we have also recorded it using the optoNCDT 1320 laser sensor [10]. Fig. 1 shows the measurement setup, with the live dummy within a rear-facing child restraint system. The obtained results for a breathing rate of 25 bpm can be seen in Fig. 2, comparing the actual displacement measured by the laser sensor, and the one recovered by the radar. It can be seen how the radar was able to precisely recover the movement. Small differences can still be perceived between the recovered signals and this is an expected effect. While the laser measures a single scatter point displacement, due to its limited resolution, the radar receives a superposition of signals reflected from many scatters located over the moving surfaces of the baby chest-wall and belly. Nevertheless, the periodic movement can still be clearly identified.

### B. *Human Tests*

For evaluating the final performance of the system, human experiments were also performed in a laboratory environment. Fig. 3 shows the measurement setup, where the subject was asked to stay seated in front of the radar, at 1.5 m distance. A wearable commercial device, named Hexoskin [11], was used as a reference for the chest-wall displacement and the actual breathing rate over time. This device has already been extensively validated for breathing estimation in different conditions [12]. The first test was a hold and release test, in which the subject was breathing for 30 seconds, holding the breath for 30 seconds (inhaled), and finally breathing again in the last 30 seconds. Fig. 4 shows the obtained chest-wall displacement over time, comparing radar data to the reference device. It can be seen the high correlation between both measurements, where breathe and hold moments can be easily identified. Additionally, the inset figure shows that, when the subject is not breathing, the residual heartbeat periodic movement becomes also clearly visible in the radar data. In the following test, the subject was asked to stay seated in front of the radar, at the same distance, and breathing normally for 10 minutes. Fig. 5 shows the final estimated values from radar and reference device. Most of the time (94.5%) the radar provides measurements within the $\pm 1$ bpm error interval, being capable of tracking the actual values even during fast variations of the breathing frequency.

The concluding tests were performed still in seated position, but now emulating different conditions of movement. The idea was to understand if small random movements from hands, arms and shoulder, which are very close the chest, could jeopardize breathing estimation. Besides being static, two other scenarios were emulated: 1) the subject was texting in the phone, and 2) the subject was typing in a keyboard, while also controlling a mouse device. In all three cases, the subject was asked to breath normally for 3 minutes, and each condition was repeated 5 times. The obtained results are summarized in Table 1, which shows the average accuracy and Root-Mean-Square Error (RMSE) for each scenario, comparing the proposed NLS estimator with both standard estimation over the DFT spectrum


Authorized licensed use limited to: Technische Informationsbibliothek (TIB). Downloaded on April 04,2025 at 12:10:30 UTC from IEEE Xplore. Restrictions apply.

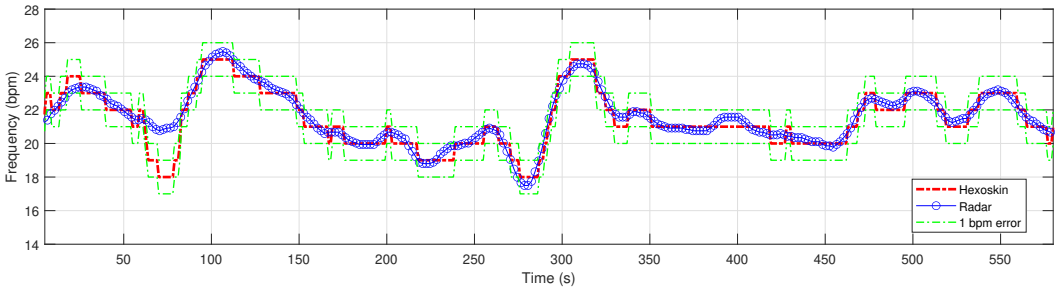


Fig. 5. Estimated values for a single 10 minutes test. The red line is the reference sensor, with the $\pm 1$ bpm error interval in green.

Table 1. Average accuracy and RMSE for different scenarios.

| Test | Accuracy (%) | | | RMSE (bpm) | | |
|---|---|---|---|---|---|---|
| | DFT | FTPR | NLS | DFT | FTPR | NLS |
| **Static** | 93.7 | 98.3 | 99.3 | 0.53 | 0.44 | 0.42 |
| **Texting** | 97.8 | 97.8 | 99.8 | 0.45 | 0.42 | 0.35 |
| **Typing** | 92.8 | 93.7 | 94.2 | 0.71 | 0.66 | 0.69 |

and the FTPR method from [2], [13], [14]. The accuracy is being calculated as the percentage of time in which the final estimation from the radar is within the $\pm 1$ bpm error interval, i.e. when the error between the radar estimation and the actual value is less than 1 bpm, the measurement counts as a correct estimation. The RMSE is defined as

$$\text{RMSE} = \sqrt{\frac{1}{N}\sum_{i=1}^{N}(\hat{B}_i - B_i)^2}, \tag{9}$$

where $\hat{B}_i$ and $B_i$ represent the reference and estimated breathing rates (in bpm) in the $i^{th}$ CPI, respectively. From the table, it can be seen how the proposed framework provides accurate and robust breathing estimation in all three conditions, with minor performance loss when texting and typing. The most challenging situation arises when moving the arms back-and-forth for controlling the mouse device. Besides overlapping identical range bins, this movement has a similar behavior as the chest-wall displacement when breathing, but with much stronger amplitudes.

## V. Conclusion

In this paper we presented our experimental results of breathing detection and estimation using a FMCW 77 GHz device. For tackling this, we proposed a complete signal processing framework using a simple and efficient NLS estimator, which was evaluated with real human data in different scenarios. Most of the time the radar provided measurements within the $\pm 1$ bpm error interval, being capable of tracking the true values even during fast variations of the breathing frequency. The final accuracy and RMSE values have shown robust and accurate estimation, outperforming standard DFT and FTPR estimation over different scenarios.

## Acknowledgment

This work was supported by the National Research Fund of Luxembourg, under the FNR Industrial Fellowship Grant for Ph.D. projects (reference 14269859).

## References

[1] M. Kebe, R. Gadhafi, B. Mohammad, M. Sanduleanu, H. Saleh, and M. Al-qutayri, "Human vital signs detection methods and potential using radars: A review," *Sensors (Switzerland)*, vol. 20, no. 5, 2020.

[2] M. Nosrati and N. Tavassolian, "High-Accuracy Heart Rate Variability Monitoring Using Doppler Radar Based on Gaussian Pulse Train Modeling and FTPR Algorithm," *IEEE Transactions on Microwave Theory and Techniques*, vol. 66, no. 1, pp. 556–567, 2018.

[3] A. De Groote, M. Wantier, G. Cheron, M. Estenne, and M. Paiva, "Chest wall motion during tidal breathing," *Journal of Applied Physiology*, vol. 83, no. 5, pp. 1531–1537, 1997.

[4] P. Stoica, R. L. Moses *et al.*, "Spectral analysis of signals," 2005.

[5] M. G. Christensen and A. Jakobsson, "Multi-pitch estimation," *Synthesis Lectures on Speech & Audio Processing*, vol. 5, no. 1, pp. 1–160, 2009.

[6] *Radar Device*, (accessed October 28, 2020). [Online]. Available: https://www.ti.com/product/AWR1642

[7] M. Zakrzewski, A. Singh, E. Yavari, X. Gao, O. Boric-Lubecke, J. Vanhala, and K. Palovuori, "Quadrature imbalance compensation with ellipse-fitting methods for microwave radar physiological sensing," *IEEE Transactions on Microwave Theory and Techniques*, vol. 62, no. 6, pp. 1400–1408, 2014.

[8] B. K. Park, O. Boric-Lubecke, and V. M. Lubecke, "Arctangent demodulation with DC offset compensation in quadrature Doppler radar receiver systems," *IEEE Transactions on Microwave Theory and Techniques*, vol. 55, no. 5, pp. 1073–1078, 2007.

[9] A. R. Diewald, J. Landwehr, D. Tatarinov, P. Di Mario Cola, C. Watgen, C. Mica, M. Lu-Dac, P. Larsen, O. Gomez, and T. Goniva, "RF-based child occupation detection in the vehicle interior," *Proceedings International Radar Symposium*, vol. 2016-June, pp. 1–4, 2016.

[10] *optoNCDT Device*, (accessed October 28, 2020). [Online]. Available: https://www.micro-epsilon.com/displacement-position-sensors/laser-sensor/

[11] *Hexoskin Device*, (accessed October 28, 2020). [Online]. Available: https://www.hexoskin.com/

[12] R. Villar, T. Beltrame, and R. L. Hughson, "Validation of the Hexoskin wearable vest during lying, sitting, standing, and walking activities," *Applied Physiology, Nutrition and Metabolism*, vol. 40, no. 10, pp. 1019–1024, 2015.

[13] M. Nosrati and N. Tavassolian, "Accurate Doppler Radar-Based Cardiopulmonary Sensing Using Chest-Wall Acceleration," *IEEE Journal of Electromagnetics, RF and Microwaves in Medicine and Biology*, vol. 3, no. 1, pp. 41–47, 2019.

[14] B. Guo, Z. Yang, Y. Cheng, and J. Zhou, "Respiratory Frequency Estimation Method Based on Periodic Features Using UWB Radar," *ICEICT*, pp. 139–143, 2021.



Authorized licensed use limited to: Technische Informationsbibliothek (TIB). Downloaded on April 04,2025 at 12:10:30 UTC from IEEE Xplore. Restrictions apply.